

Reduction of chaotic particle transport driven by drift waves in sheared flows

F. A. Marcus, I. L. Caldas, Z. O. Guimarães-Filho, P. J. Morrison, W. Horton et al.

Citation: *Phys. Plasmas* **15**, 112304 (2008); doi: 10.1063/1.3009532

View online: <http://dx.doi.org/10.1063/1.3009532>

View Table of Contents: <http://pop.aip.org/resource/1/PHPAEN/v15/i11>

Published by the [American Institute of Physics](#).

Related Articles

Two-dimensional quasi-double-layers in two-electron-temperature, current-free plasmas

Phys. Plasmas **20**, 023502 (2013)

Binding energy levels of a slowly moving ion in dusty plasmas

Phys. Plasmas **20**, 023701 (2013)

Plasma electron source for the generation of wide-aperture pulsed beam at forevacuum pressures

Rev. Sci. Instrum. **84**, 023301 (2013)

Theory of magnetic field line random walk in noisy reduced magnetohydrodynamic turbulence

Phys. Plasmas **20**, 012308 (2013)

Magnetic stochasticity and transport due to nonlinearly excited subdominant microtearing modes

Phys. Plasmas **20**, 012307 (2013)

Additional information on Phys. Plasmas

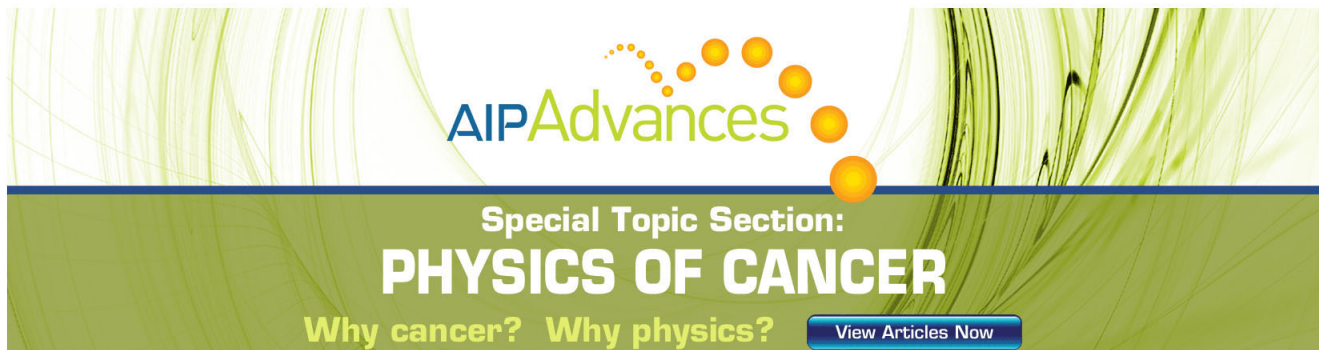
Journal Homepage: <http://pop.aip.org/>

Journal Information: http://pop.aip.org/about/about_the_journal

Top downloads: http://pop.aip.org/features/most_downloaded

Information for Authors: <http://pop.aip.org/authors>

ADVERTISEMENT



AIP Advances

Special Topic Section:
PHYSICS OF CANCER

Why cancer? Why physics? [View Articles Now](#)

Reduction of chaotic particle transport driven by drift waves in sheared flows

F. A. Marcus,¹ I. L. Caldas,¹ Z. O. Guimarães-Filho,^{1,a)} P. J. Morrison,² W. Horton,² Yu. K. Kuznetsov,¹ and I. C. Nascimento¹

¹*Institute of Physics, University of São Paulo, C.P. 66318, 05315-970 São Paulo, São Paulo, Brazil*

²*Department of Physics and Institute for Fusion Studies, The University of Texas at Austin, Austin, Texas 78712, USA*

(Received 2 June 2008; accepted 9 October 2008; published online 7 November 2008)

Investigations of chaotic particle transport by drift waves propagating in the edge plasma of tokamaks with poloidal zonal flow are described. For large aspect ratio tokamaks, the influence of radial electric field profiles on convective cells and transport barriers, created by the nonlinear interaction between the poloidal flow and resonant waves, is investigated. For equilibria with edge shear flow, particle transport is seen to be reduced when the electric field shear is reversed. The transport reduction is attributed to the robust invariant tori that occur in nontwist Hamiltonian systems. This mechanism is proposed as an explanation for the transport reduction in Tokamak Chauffage Alfvén Brésilien [R. M. O. Galvão *et al.*, *Plasma Phys. Controlled Fusion* **43**, 1181 (2001)] for discharges with a biased electrode at the plasma edge. © 2008 American Institute of Physics. [DOI: 10.1063/1.3009532]

I. INTRODUCTION

A critical obstacle to improved fusion plasma confinement in tokamaks is the presence of electrostatic turbulence at the plasma edge.^{1–3} This turbulence produces anomalous particle and energy transport at the plasma edge that is much higher than the values predicted by neoclassical transport theory for transport by collisions in toroidal geometry.^{3,4} Electrostatic turbulence is associated with drift waves that propagate in the poloidal direction and are driven by equilibrium radial gradients.³ Experiments indicate that at the plasma edge the observed anomalous particle transport is mainly caused by the particle $\mathbf{E} \times \mathbf{B}$ drift.^{5–7}

Several experiments show that particle transport can be reduced by changing the electric field radial profile at the plasma edge.^{8,9} One experimental procedure to achieve this reduction is the biasing scheme.^{8–13} The effect of electric field biasing observed in several machines in general leads to a strongly varying radial electric field, E_r , as a function of radius and a resulting sheared $\mathbf{E} \times \mathbf{B}$ flow, giving rise to improved confinement properties.^{14–16}

Moreover, since the discovery of the transition from the low confinement mode (L-mode) to the high confinement mode (H-mode),¹⁷ a link between E_r and the formation of edge transport barriers in toroidal devices has been experimentally and theoretically recognized. Thus, electrode biasing has contributed significantly to the understanding of the H-mode phenomenon and the effect of E_r on plasma transport. Furthermore, the influence of the E_r -profile on the L-H transition and on the reduction of transport confirms that turbulence is the main cause of energy and particle losses.

The observed particle transport reduction has been at-

tributed to equilibrium shear flow that decorrelates the turbulence, and it is an experimental fact that shear is coincident with spectral broadening and transport reduction.^{5,7} This early work on the tokamak motivated the idea that shearing of turbulent eddies by the $\mathbf{E} \times \mathbf{B}$ flow velocity is a universal mechanism for stabilizing and decorrelating turbulence in plasmas, as discussed in Refs. 18–22. In these references, this mechanism is implemented by invoking a passive scalar ion density, and a reduced diffusion coefficient is obtained by a renormalized turbulence theory that is akin to quasilinear theory. Such a theory requires resonance overlap and the concomitant destruction of invariant surfaces, which is a reasonable assumption in regions with high shear. However, when the shear flattens, quasilinear theory may not be applicable and wave dynamical effects may dominate. Recent experiments in the large plasma device (LAPD), in its long (17 cm) cylindrical plasma, with biasing to control E_r , show a density transport barrier forming where the shear vanishes, in the case where drift waves are active.²³ This is in agreement with barriers to transport that are observed in rotating fluid experiments at the shearless point of zonal flows.^{24,25} In other experiments on the LAPD, where the Kelvin–Helmholtz instability is active, barriers are not seen near strong shear flow regions, but again appear where the shear is flattened.²³ Thus, it is important to investigate the role of drift-wave dynamics,²⁶ in addition to broadband turbulence, on transport.

The objective of this paper is to investigate particle transport by drift waves propagating in the plasma edge of tokamaks with $\mathbf{E} \times \mathbf{B}$ poloidal flow. A simple Hamiltonian theory with chaotic dynamics is proposed and used to interpret transport data. The Hamiltonian theory has two important features that affect the transport, one that facilitates and one that inhibits. The first feature occurs when the electric

^{a)}Author to whom correspondence should be addressed. Electronic mail: zwinglio@if.usp.br.

field at the edge gives rise to an $\mathbf{E} \times \mathbf{B}$ velocity that matches the phase velocity of one of the drift waves. When this resonance occurs, the equilibrium electric field is dwarfed by that of the drift wave and a grid of convective cells or island structures is produced that locally traps particles. Such a phase space configuration is structurally unstable to perturbation; for example, if another drift wave is added large scale chaotic transport ensues.

The second feature occurs for equilibrium electric field profiles that are not monotonic, as is the case with zonal flows. When this occurs, the Hamiltonian system violates a condition known as the twist condition,²⁷ because there is a point of vanishing flow shear. It was demonstrated in a sequence of works^{24,25,28–32} that Hamiltonian systems that violate the twist condition in a generic way, so-called nontwist Hamiltonian systems, possess *robust* invariant tori or barriers that inhibit transport. This applies, for example, to systems that describe particle transport in zonal shear flows in fluids and plasmas, like that of interest here, and to Hamiltonian systems that describe magnetic field lines in tokamaks with reverse shear. The result that shearless tori are robust and inhibit transport is in direct contradiction to a claim of Ref. 33, a claim that early on was brought into question in Ref. 34. Nontwist systems have been further explored in a variety of transport models, e.g., Refs. 35–38. Here we give experimental evidence that nontwist inhibits transport. It should be noted that even after tori in nontwist systems are broken, their remnants can still inhibit transport because there exist regions of stickiness where trajectories linger.

We take as a starting point the nonintegrable Hamiltonian model of Ref. 39, which might be reasonable for describing large aspect ratio tokamaks. With this model, the total flow, formed by the equilibrium flow and two dominant resonant drift waves, is not turbulent, yet particle trajectories are chaotic²⁶ and thus can give rise to transport. In Sec. II, we describe the relevant features of this two-wave model needed for our study in this paper, following Refs. 26 and 40–42.

In Sec. III, we study the influence of the radial electric field profile on the convective cells and transport barriers created by the nonlinear dynamical interaction between the poloidal flow and the waves. For equilibria with reverse shear flows, our results show that the particle transport can be reduced by modifying the electric field profile. In Sec. IV, we use our simple model to interpret recent tokamak experiments performed for studying the transport reduction caused when a biased electrode is inserted into the plasma edge region. Parameters for equilibrium and fluctuating electric field radial profiles are extracted from Tokamak Chauffage Alfvén Brésilien (TCABR) data,⁴³ and the model thus obtained is used to calculate transport during standard Ohmic and improved confinement regimes obtained in this tokamak by biasing. A good prediction for the bias voltage necessary for improved confinement is obtained, a prediction consistent with the existence of robust tori. Finally, in Sec. V, we summarize our results and discuss possible limitations.

II. DRIFT WAVE DRIVEN TRANSPORT

In this section we investigate particle transport induced by electrostatic waves propagating in the poloidal direction in a magnetized plasma with a constant toroidal magnetic field $\mathbf{B} = B_0 \hat{\mathbf{e}}_z$. The drift velocity of the guiding centers is given by $\mathbf{v} = \mathbf{E} \times \mathbf{B} / B^2$. We assume particles move at this velocity; consequently they satisfy

$$\dot{x} = -\frac{1}{B_0} \frac{\partial \phi}{\partial y} \quad \text{and} \quad \dot{y} = \frac{1}{B_0} \frac{\partial \phi}{\partial x}, \quad (1)$$

where $\mathbf{E} = -\nabla \phi(x, y, t)$. Defining $H(x, y, t) = \phi / B_0$, and identifying x as the canonical momentum and y as its conjugate coordinate, we see Eq. (1) is a Hamiltonian system. Consistent with the simplicity of our model, it is not unreasonable to assume Cartesian coordinates, which are more justified for large aspect ratio tokamaks. We identify x and y as the radial and poloidal coordinates, respectively.

We posit an electrostatic potential of the form²⁶

$$\phi(x, y, t) = \phi_0(x) + \sum_i A_i \sin(k_{x_i} x) \cos(k_{y_i} y - \omega_i t), \quad (2)$$

which is composed of a background equilibrium electrostatic potential, $\phi_0(x)$, with the superposition of a collection of drift waves propagating in the poloidal direction.

Neglecting the drift waves, the flow velocity in the poloidal direction is represented by

$$v_E(x) = \frac{1}{B_0} \frac{d\phi_0}{dx}, \quad (3)$$

which we will assume is perturbed by two drift waves, the minimum number necessary for chaos. It is convenient to boost to a frame rotating in the poloidal direction at the phase velocity of one of the waves, and this is achieved by the following canonical transformation:

$$x = x' \quad \text{and} \quad y = y' - \frac{\omega_1}{k_{y1}} t = \frac{\partial F_2(x', y, t)}{\partial x'},$$

where the generating $F_2(x', y, t) = x'(y - u_1 t)$ with $u_1 = \omega_1 / k_{y1}$ being the phase velocity of the first wave. In the new coordinates (omitting the primes) the Hamiltonian becomes

$$H(x, y, t) = \phi_0(x) - u_1 x + A_1 \sin(k_{x1} x) \cos(k_{y1} y) + A_2 \sin(k_{x2} x) \cos[k_{y2}(y - ut)], \quad (4)$$

where $u = \omega_2 / k_{y2} - \omega_1 / k_{y1}$ is the phase velocity difference between the two waves.

If only one wave is present ($A_2 = 0$), the Hamiltonian is

$$H_1(x, y) = \phi_0(x) - u_1 x + A_1 \sin(k_{x1} x) \cos(k_{y1} y) \quad (5)$$

and the system is integrable; there is no chaos in the phase space and particles are confined to curves of constant H_1 . In the case of constant electric field, there is only a single relevant dimensionless parameter, the trapping parameter $U \sim v_E - u_1$.^{26,40,42} This name derives from the fact that when the trapping parameter vanishes there is a resonance effect because the wave phase velocity matches the background drift velocity, the first feature alluded to in Sec. I. This reso-

nance then opens the grid of islands that traps orbits. The system with $U \equiv 0$ has no shear and is an example of a *no twist* (distinct from nontwist) Hamiltonian system.

Because we are also interested in electric fields that have spatial variation we will refer to the *trapping profile* defined by

$$U(x) = \frac{1}{A_1 k_{x1}} \left[\frac{d\phi_0(x)}{dx} - u_1 B_0 \right] = \frac{B_0}{A_1 k_{x1}} [v_E(x) - u_1], \quad (6)$$

where again A_1 , k_{x1} , and u_1 are the peak-to-peak amplitude in V, the radial wave number in m^{-1} , and phase velocity in m/s of the dominant edge mode, $v_E(x)$ is the radial profile of the poloidal flow velocity from the E_r radial electric field and B_0 the toroidal field is in T.

Experiments have shown that the plasma edge transport is high when the condition $U \sim 0$ is satisfied.⁷ We show in the next section that the trapping profile is important for characterizing the behavior of phase space and, consequently, the radial transport of particles. When a shearless point exists, a point where $U' = 0$, then we have a nontwist Hamiltonian system with the second feature alluded to in Sec. I, and we expect the appearance of robust tori or sticky regions in its vicinity.

The onset of chaos in the phase space takes place when the second wave is added. The existence of transport will be confirmed by calculating the diffusion coefficient from the orbits. For the calculation of the finite time local diffusion coefficient we consider the nondimensional equation of the following form:⁴⁰

$$D'(t') = \frac{1}{2t'N} \sum_{i=1}^N [x'_i(t') - x'_i(0)]^2, \quad (7)$$

which is related to the diffusion coefficient, measured in m^2/s , by

$$D(t) = \frac{r_0 E_0}{B_0} D'(t'), \quad (8)$$

where r_0 is the plasma radius in m, E_0 is the equilibrium electric field in V/m, and B_0 is the magnetic field in T. A more effective transport estimate would require a global description of turbulence as considered, for example in Ref. 44.

III. SHEAR FLOW AND TRANSPORT

In this section we analyze both constant and variable U . First, suppose the equilibrium electrostatic potential at the plasma edge is linear,^{39,42} $\phi_0(x) = -E_0 x + \text{const}$, where E_0 is the uniform equilibrium electric field. Understanding the phase space of this linear potential is important for later consideration of nonuniform trapping profiles. Thus, the trapping parameter is given by $U = -(E_0 + u_1 B_0) / A_1 k_{x1}$. Because the aim of this work is to study the effect of the electric field on radial transport, we fix all parameters except E_0 and suppose this quantity is responsible for changes in U .

In Fig. 1, the phase space is shown for three different values of the trapping parameter for a single wave, i.e., $A_2 = 0$. Figure 1(a) depicts the flow configuration for $U = 0$, where it is seen that a grid of islands or convective cells

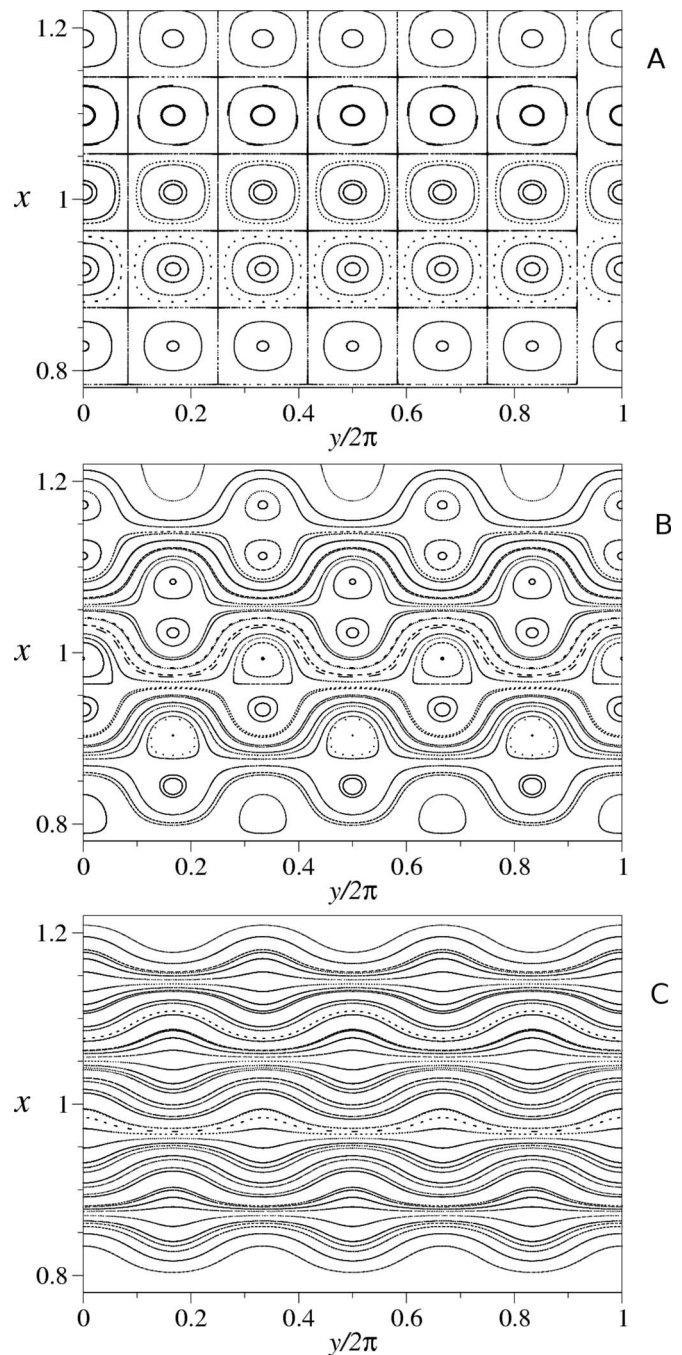


FIG. 1. Phase space plots for (a) $U=0$, (b) $U=0.5$, and (c) $U=1.5$ with a single wave ($A_2=0$).

covers all of phase space. Each basic unit cell has two hyperbolic points and two elliptic points. Notice that there are separatrix lines in the vertical and horizontal directions, and one expects that a slight perturbation of these will allow particles to move large distances in both the poloidal and radial directions.

In Fig. 1(b), $U=0.5$ and the phase space is composed of islands and open flow lines that correspond to particles circulating around the torus in the poloidal direction. Thus, some particles circulate around the elliptic points, while others make complete circuits in the poloidal direction. Upon increasing the electric field magnitude so $U=1.5$, we see in

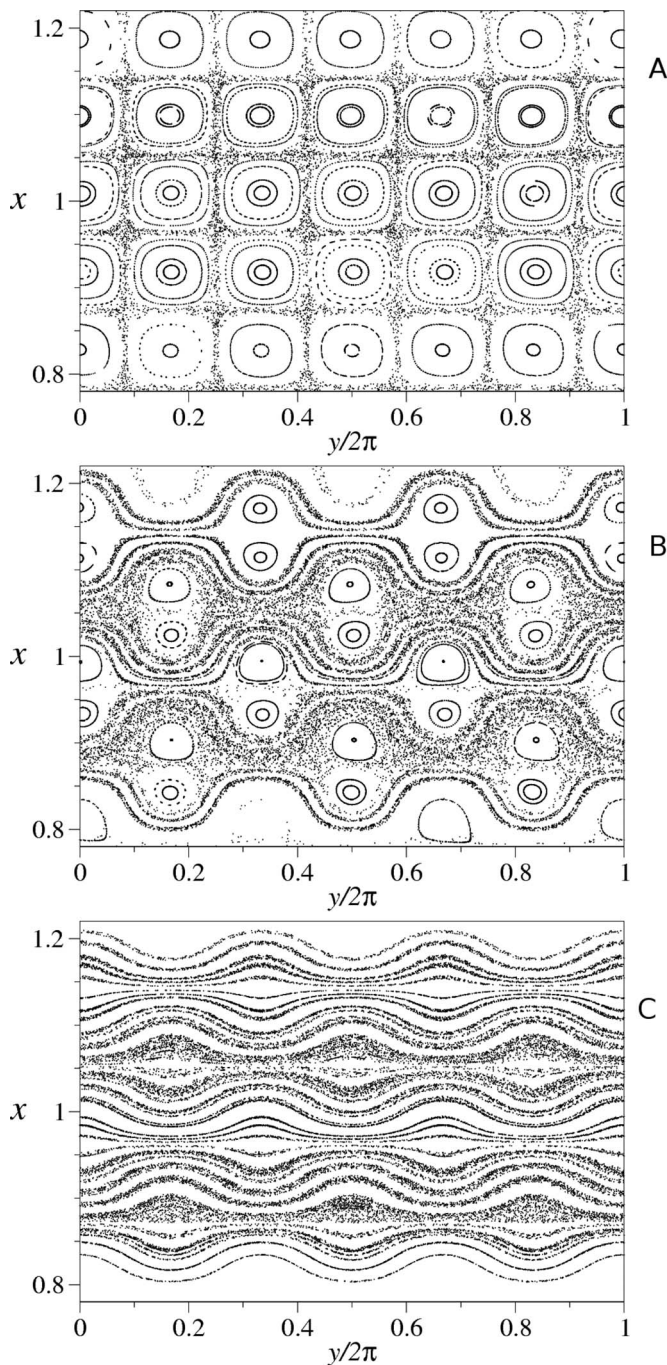


FIG. 2. Surface of section plots for (a) $U=0$, (b) $U=0.5$, and (c) $U=1.5$ with the inclusion of a second wave with amplitude ratio $A_2/A_1=0.1$.

Fig. 1(c) that the phase space is now characterized by open flow lines. Open flow lines are the invariant tori that are barriers to transport.

Figure 2 shows surfaces of section that depict how the addition of the second wave changes the phase space for the three cases considered in Fig. 1, building upon the earlier work of Refs. 41, 42, and 45. We suppose the second wave appears with the ratio of amplitudes given by $A_2/A_1=0.1$ and we strobe at the period of the second wave. Figure 2(a) shows how the transport depends on the grid of the first wave islands and the second wave amplitude. Upon comparison to Figs. 2(b) and 2(c), observe that the chaos is more wide-

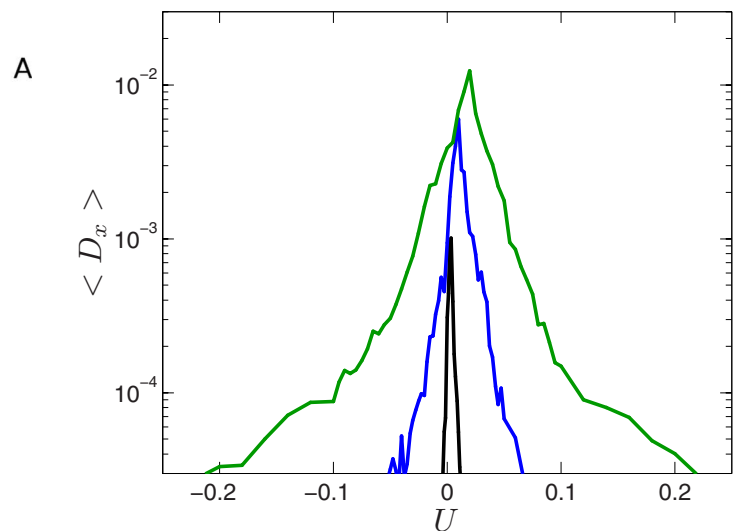


FIG. 3. (Color online) Diffusion coefficient as a function of trapping parameter U for different values of the wave amplitude ratio A_2/A_1 : $A_2/A_1=0.1$ in black, $A_2/A_1=0.4$ in blue, and $A_2/A_1=0.8$ in green. The numerical simulation shows that the radial transport is largest for $U=0$, increases with A_2/A_1 , and decreases with increasing $|U|$.

spread for Fig. 2(a), where $U=0$, the separatrices opening up into chaotic channels, and orbits are able to traverse large distances in phase space. The second wave allows particles to move within the separatrix regions and then jump one or more cells until being temporarily trapped in the vicinity of another elliptic point. Thus, the transport is characterized by both trapping and flight events (see, e.g., Ref. 28).

When $U=0.5$, Fig. 2(b), we see that the chaos is for the most part localized. The open flow lines widen, but there is no net transport in the radial direction. Similarly, for $U=1.5$, Fig. 2(c), particles are seen to move on open flow lines in poloidal circuits.

To understand the significance of the trapping parameter for transport, with the presence of the second wave, we calculated the diffusion coefficient $\langle D_x \rangle$ as a function of U for different values of the ratio A_2/A_1 . Examination of Fig. 3 near $U=0$ shows that the transport is clearly highest for this trapping parameter value, increases and becomes broader for augmenting A_2/A_1 , and diminishes for larger values of $|U|$. For larger values of $|U|$, barriers exist and in actual fact the net global radial transport must be identically zero. The diffusion dependence on U is a dynamical consequence of the resonant waves propagating with phase velocity near the plasma flow velocity ($U \sim 0$). In fact, the observed particle trapping regions, described as barriers, increase with $|U|$. Figure 3 shows that the diffusion coefficients drops drastically away from resonance. Thus, from the present model one expects high diffusion for resonant waves. However, if the resonance condition is not fulfilled, other effects may be dominant. The presence of a barrier for $|U| \geq 1$ is another dynamical effect that inhibits the diffusion. Diffusion also depends on the resonant radial wavenumber. As the trapping parameter U is proportional to the inverse of the resonance radial wave number [cf. Eq. (6)], its values are high for large radial structures (with small wave numbers) and, consequently, the contribution of these structures to the resonant

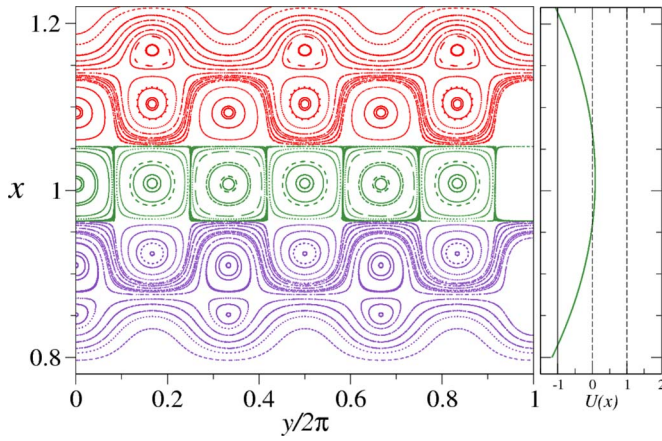


FIG. 4. (Color online) For a nonmonotonic electric field profile, the three phase space configurations of Fig. 1 are observed at different positions. For the chosen values of A , B , and C of Eq. (9), $U_{\max}=0.1$.

transport considered in this work is lower than the small structure contribution.

For the small tokamak TBR,⁴⁶ measurements obtained with electrostatic probes show that the potential at the plasma edge is almost linear. Experimental power spectrum analysis of TBR data⁴⁷ suggests a frequency of 30 kHz for the first wave and 18 kHz for the second.⁴⁸ Also, data suggest that $A_2/A_1 \approx 0.8$ and $U \approx 0$. With these choices, the estimated diffusion coefficient is $D \sim 2.0 \text{ m}^2/\text{s}$,⁴⁹ which is in order of magnitude agreement with the diffusion coefficient of $D=0.5 \text{ m}^2/\text{s}$ measured in TBR.⁵⁰ This is reasonable agreement between the model and the experimental data, given that the model is limited to only resonant chaotic transport.

In other tokamak discharges, in particular, the ones considered in the next section, the electrostatic potential at the plasma edge is not a linear function. Thus, we consider the following form for the radial dependence of the potential:

$$\phi_0(x) = Ax^3 + Bx^2 + Cx + D, \quad (9)$$

and consequently, the trapping profile is given by

$$U(x) = \frac{1}{A_1 k_{x1}} (3Ax^2 + 2Bx + C - u_1 B_0). \quad (10)$$

For this profile, there exists a shearless point and, therefore, the system with the Hamiltonian H_1 of Eq. (5) is a nontwist Hamiltonian system. The same holds true for the system with Hamiltonian H of Eq. (4) provided the second wave is a perturbation. Because of the existence of the extremal point, the system without the presence of the waves corresponds to a pure zonal flow with only the open flow lines. Thus, as discussed in Sec. I, when the waves are included, we expect the appearance of regions with robust tori that provide barriers to transport.

It is important to distinguish the two features of our discussion. The resonance feature occurs when $U=0$, while the nontwist feature occurs when $U'=0$ and $U \neq 0$. However,

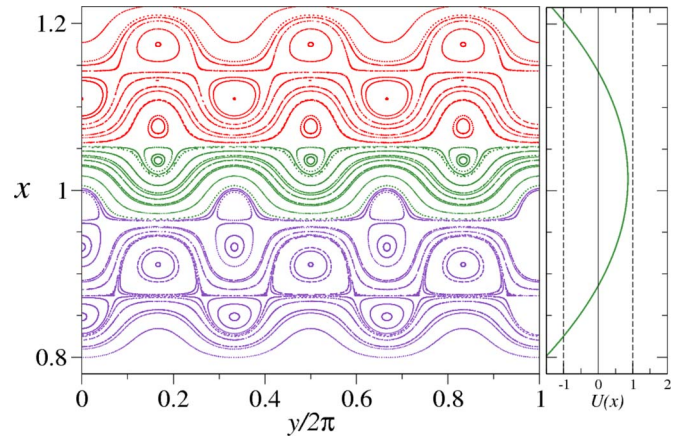


FIG. 5. (Color online) Values of A , B , and C in Eq. (9) are chosen to shift the maximum of the parabola to $U=0.8$. The islands and the circulating flow rearrange, in comparison to Fig. 4. Note that the islands that were located near the edge at $x=0.85$ have change to circulating flow.

there is also a degenerate case where both $U'=0$ and $U=0$, which we will not discuss in detail.

Figure 4 depicts the curves of constant H_1 . Notice that all three configurations presented in Fig. 1 occur here but in different regions of the same phase space. The trapping profile U is plotted on the right-hand side for particular values of the parameters A , B , and C , and this can be used to explain the behavior in the different regions. Islands occur near the edge, $x \approx 1$, a region where the trapping profile is small near $U'=0$. In this case, the grid of islands dominates over the robust tori and one expects particle transport to be high at the edge when the second wave is added.

With the connection between the trapping parameter U and the electric field in mind, we change the values of A , B , and C , in such a way that the maximum of the trapping profile reaches $U_{\max}=0.8$. This is enough to change the configuration of the phase space, as can be seen in Fig. 5. With these parameter values, islands appear inside the plasma ($x < 1$). At the plasma edge ($x=1$), there are only the open flow lines corresponding to circulating poloidal flow. As a consequence, we expect the presence of robust tori when the second wave is added, and, concomitantly, diminished chaotic transport at the plasma edge in the vicinity of the shearless point.

In Fig. 6(a), the single-wave phase space is depicted with parameter values giving rise to barriers near the shearless point at $x=1.0$, which occur for a trapping profile that has a maximum value of $U_{\max}=1.3$. These barriers describe a zonal flow of circulating particles. When the second wave is added, Fig. 6(b), the transport depends on both the grid structure of the first wave and the second wave amplitude. The zonal flow barriers, particles above [top set of curves (red online)] and below [bottom set of curves (blue online)] the zonal flow [middle set of curves (green online)] do not intermix because of the robust tori, despite the appearance of chaos. Particles at the edge circulate in the poloidal direction with no net radial transport.

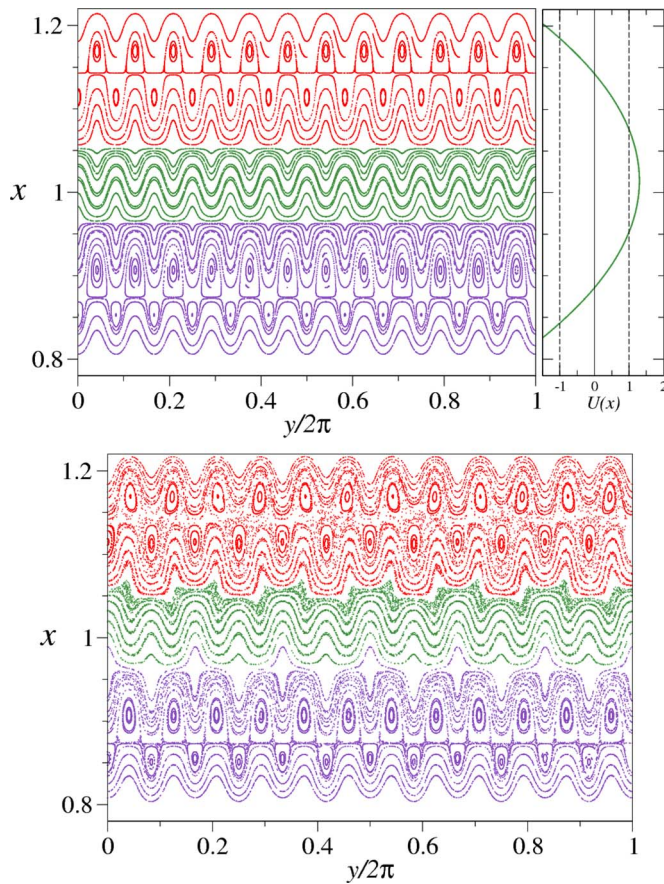


FIG. 6. (Color online) Phase space plots with parameter values chosen to give a radial electric field with large maximum trapping profile of $U_{\max} = 1.3$. The upper figure shows circulating edge particles [middle set of curves (green online)] in the presence of a single wave. The lower figure depicts the effect of inclusion of the second wave. Observe the island structure becomes chaotic, but the particle barriers are robust and particles in red and blue do not cross the green flow region.

IV. CHANGING THE E_r -PROFILE IN TCABR

Of the different methods developed to perturb tokamak plasmas, the insertion of a biased electrode is one that acts directly on the radial electric field at the plasma edge. In Sec. III, we described how different phase space configurations arise from different electric field profiles, and the relationship between phase structure and radial transport. Without prior knowledge of the specifics of the bias field in the experimental results, we applied the model described above to both biased and unbiased discharges of the tokamak TCABR and predicted a value of the bias voltage that turned out to be close to the voltage observed for the onset of reduced transport from the turbulence.

Our first task is to extract from TCABR data the phase velocity of the first (dominant) wave. To do this we use measurements obtained by a set of two Langmuir probes separated in the poloidal direction by 0.4 cm,¹¹ and the power spectrum is obtained with this two point probe technique.⁵¹ The result for $r=18$ cm, which is the radius of the plasma edge, is depicted in Fig. 7, where the spectrum is plotted as a function of frequency and wavenumber. As can be seen, the frequency range is large, but a peak occurs for a frequency of

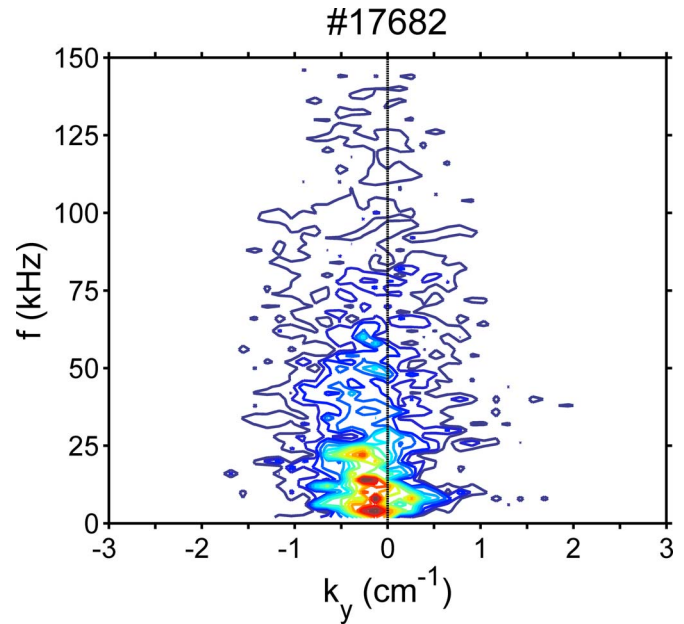


FIG. 7. (Color online) Power spectrum $S(k, f)$ obtained from shot 17682 at the plasma edge $r=18$ cm of TCABR.

about $f_1=20$ kHz and poloidal wavenumber of about $k_{y1}=0.3$ cm^{-1} . We take these values for our first wave.

To determine the parameters A, B, C, D of Eq. (9), we use probe measurements of mean values of the floating potential for 57 shots in TCABR at several radial positions near the plasma edge and scrap-off layer regions. This was done for both simple Ohmic discharges and discharges with a biased electrode. The confinement improvement due to edge biasing in TCABR was described in Ref. 11. In Fig. 8, results for both Ohmic discharges (continuous green) and the biased discharges (dashed blue) are shown. Each point of the figure is obtained from an average over several similar shots. The error bars measure the expected uncertainty in the average values. Continuous curves are fit to the data to determine the

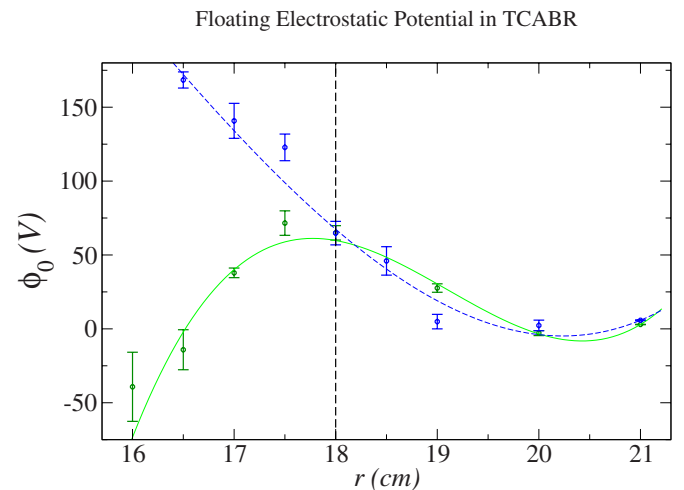


FIG. 8. (Color online) Floating electrostatic potential for Ohmic (continuous green) and biased (dashed blue) discharges. The plasma lies to the left of the boundary located at $r=18$ cm.

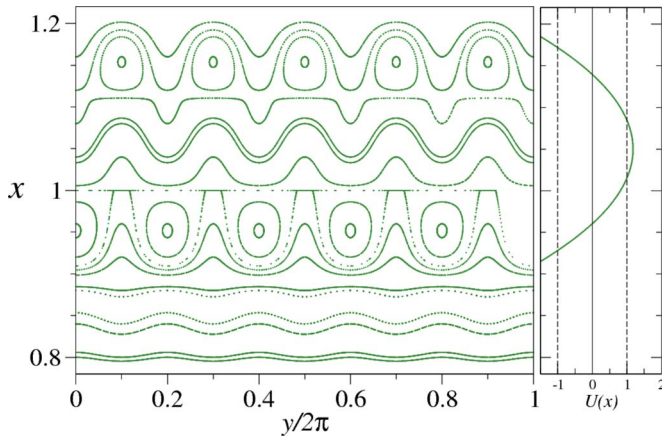


FIG. 9. (Color online) Phase space with the trapping profile for Ohmic discharges in TCABR.

parameter values. Notice that because the plasma edge is located at $r=18$ cm, the Ohmic discharges have a monotonic profile within the plasma near the edge.

With the parameter values for the potential and first wave in hand, we can plot the phase space energy curves corresponding to the Hamiltonian H_1 . This is done in Fig. 9 for Ohmic discharges where, as in Sec. III, we plot the trapping profile on the right. Here, x is measured in units of the plasma radius, so $x=1$ corresponds to the plasma edge. In this figure it is seen that $U_{\max}=1.17$ and this occurs outside the plasma at $x=1.05$. Thus, as noted above, the electrostatic potential is monotonic and nearly linear inside the plasma.

In Fig. 10, we plot the curves of constant H_1 for the biased discharges. Observe that $U_{\max}=1.61$ occurs right at the plasma edge, $x=1.0$, and consequently there are open flow lines just inside the plasma. We expect some of these lines to survive when the second wave is added, i.e., we credit the improved confinement to the presence of the robust tori of the nontwist Hamiltonian system in the shearless region.

Measurements on tokamaks^{5,7} show that the mean wave phase velocity is close to the drift velocity v_E , indicating that $U \sim v_E - u_1 \sim 0$. Employing this result, we first obtain an es-

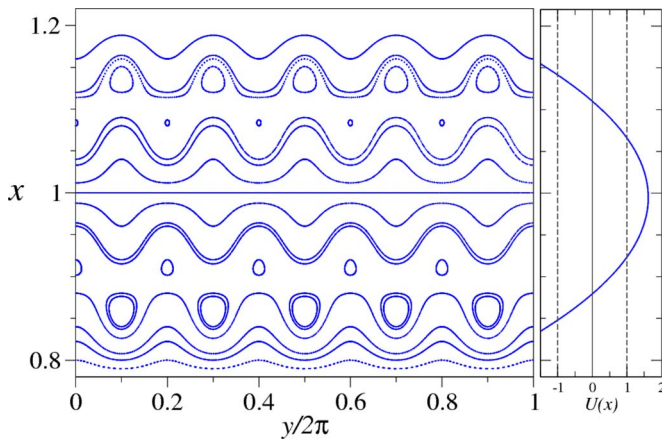


FIG. 10. (Color online) Phase space with the trapping profile for biased discharges in TCABR.

imate for the potential in TCABR for unbiased discharges. Using the TCABR parameters of $f_1=20$ kHz, $k_{y1}=0.3$ cm⁻¹, the phase wave velocity $u_1=2\pi f_1/k_{y1} \cong 4.2$ km/s. Also, in the TCABR experiments under consideration $B_0=1.1$ T. Using $E=\Delta\phi_0/\Delta x$, we obtain $\Delta\phi_0=u_1 B_0 \Delta x$ for the potential difference between two points separated by Δx at the resonance condition observed at the plasma edge, consistent with the profiles of Figs. 8 and 9.

Now we estimate the electrostatic electrode potential that is necessary to create barriers, i.e., to create robust tori near the shearless point near the plasma boundary. For biased discharges, the potential ϕ_0 that occurs in Eq. (6) is taken to be the sum of the unbiased potential ϕ_0 and the potential difference, ΔV , of the electrode relative to the grounded limiter. When the plasma is biased, the electrode is located inside the plasma at a position $\Delta x=1.5$ cm from the limiter. Thus, the relevant trapping profile is

$$U_b = \frac{1}{A_1 k_{x1}} \left[\frac{d\phi_0}{dx} - u_1 B_0 + \frac{\Delta V}{\Delta x} \right].$$

Because the plasma tends to select $d\phi_0/dx - u_1 B_0 \approx 0$, we obtain

$$U_b \approx \frac{1}{A_1 k_{x1}} \frac{\Delta V}{\Delta x}.$$

Setting $U=1$ and using $A_1=50$ V, a value extracted from the power spectrum data, and $k_{x1} \sim 5k_{y1}$, a typical value for the scale of variation in the radial direction, we obtain $\Delta V=120$ V. Experimental results, obtained independently from our calculations, show a value of the bias potential needed for significantly reducing transport to be in the range of 80–100 V, in good agreement with our estimate. This can be seen in Fig. 11 that shows the time profiles of fluctuating ion saturation current at the SOL ($r/a=1.05$) in four similar discharges with different bias rise times. This figure suggests that these fluctuations decrease as soon as a bias voltage threshold of about 100 V is reached. The reduction of the ion saturation current at the SOL is evidence for the barrier formation due to the biasing in TCABR.¹¹

We interpret the 120 V shift by appealing to Fig. 10. At this bias voltage, phase space looks as in this figure, with robust tori that act as barriers to transport lying inside the plasma edge. The bias potential displaces inward the resonant islands that occur for $U \approx 0$, and this, we suggest, is enough to reduce the radial transport.

In Fig. 12 we present experimental results that show the enhancement of the theoretically predicted barriers created when $|U| \geq 1$. This figure depicts the E-spectral contribution to the radial transport driven by turbulent flux in the scrape-off layer for four similar discharges. For each of these discharges the bias was activated at a time of 70 ms, as indicated in the figure, with values of the bias potential set to 0, 90, 170, and 250 V.

Figure 12(a) shows the unperturbed stationary intermittent transport during the analyzed time interval without biasing. In Figs. 12(b)–12(d) we see the transport reduction as the bias potential is increased, from 90 to 250 V, as indicated in (e). To quantify this transport reduction we compare

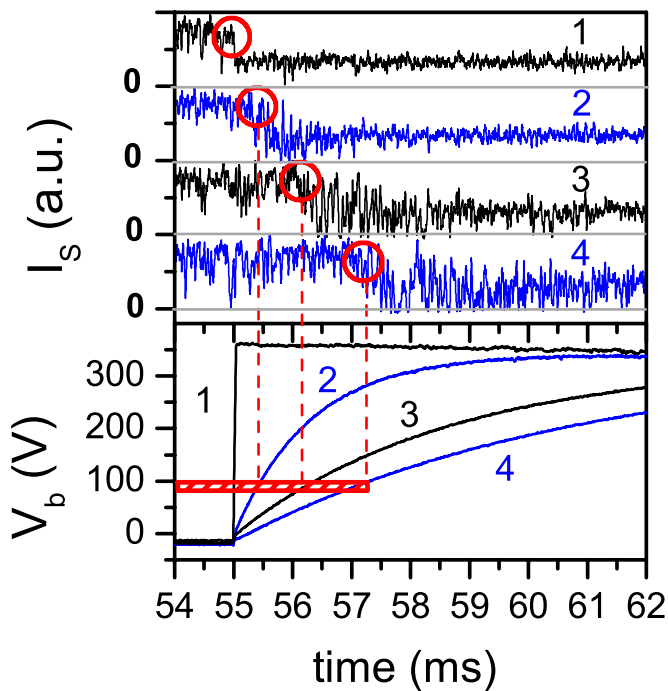


FIG. 11. (Color online) Time profiles of the mean ion saturation current measured at the SOL (I_S) and the bias voltage (V_b) applied during four similar plasma discharges of the TCABR tokamak. Mean value of the ion saturation current is calculated by averaging the time interval of 20 μ s.

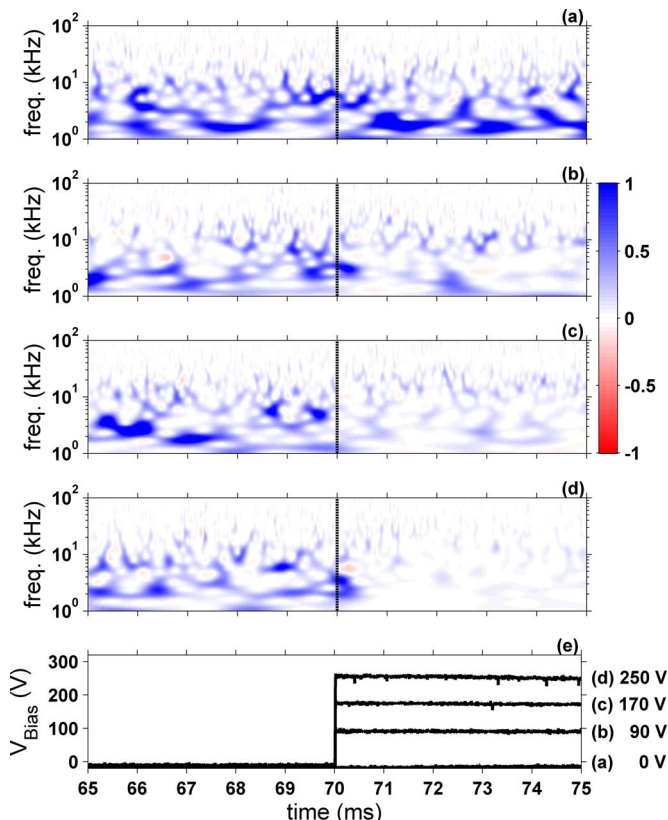


FIG. 12. (Color online) E-spectral contribution of radial transport driven by turbulent flux in the scrape-off layer for four similar discharges. From top to bottom: (a) 0 V; (b) 90 V; (c) 170 V; (d) 250 V; and (e) bias potential.

the time averaged transport integrated during 4 ms before and after the bias activation. The ratio between these two values are 0.6, 0.2, 0.1 for bias potentials of 90, 170, and 250 V, respectively. For bias potentials below 80 V, transport reduction is small (Fig. 11), and this lends credence to our assertion that the robust tori are responsible for the reduction.

V. CONCLUSIONS

In this paper we investigated chaotic particle transport by drift waves propagating in the edge plasma of tokamaks with poloidal zonal flow, by means of a Hamiltonian two-wave model. For a sheared flow with a nonuniform electric field, we described how the local particle transport changes as a function of radial position, and we showed how a modification of the radial electric field profile can be used to control transport. The trapping profile U was seen to characterize the confinement type, and that nonmonotonic profiles give rise to robust tori that inhibit transport. We investigated the dependence of transport on the amplitudes of the drift waves for given frequencies, wavenumbers, and radial electric field profiles.

For a linear electrostatic potential we obtained the diffusion coefficient for the Brazilian tokamak TBR in reasonable agreement with experimental data, lending evidence that the drift waves are important for particle transport. Furthermore, we proposed that robust tori are responsible for the transport reduction in the TCABR tokamak when a biased electrode is at the plasma edge, and this led to a good prediction for the bias voltage of the electrode.

There are many limitations of our model with simple drift wave physics and simple geometry. Chaotic advection in specified wave fields neglects the self-consistency of real turbulence, which might be expected to increase transport. However, this is not entirely clear because in some systems self-consistency can actually reduce the effective number of degrees of freedom⁵² and therefore reduce transport. The extraction of the two waves to model the observed spectrum is another limitation—a more complete model would include waves together with broadband turbulence. With a spectrum of waves, robust tori are no longer absolute barriers, however one expects that their presence or their remnants will still inhibit transport. So, obviously more work is required to firmly establish that this simple model actually captures the key physics of the transition from the low to high confinement states of the plasma. However, the results obtained are surprisingly good, being better than order of magnitude accurate, and it may just be that we have captured the dominant effects.

ACKNOWLEDGMENTS

We would like to thank D. del Castillo-Negrete for fruitful discussions.

This work was supported by FAPESP, CNPq, and CAPES. Two of us (P.J.M. and W.H.) were supported by U.S. Department of Energy Contract No. DE-FG03-96ER-54346.

- ¹J. D. Callen, B. A. Carreras, and R. D. Stambaugh, *Phys. Today* **45** (1), 34 (1992).
- ²R. D. Hazeltine and S. C. Prager, *Phys. Today* **55** (7), 30 (2002).
- ³W. Horton, *Rev. Mod. Phys.* **71**, 735 (1999).
- ⁴C. Hidalgo, *Astrophys. Space Sci.* **292**, 681 (2004).
- ⁵C. P. Ritz, R. D. Bengtson, S. J. Levinson, and E. J. Powers, *Phys. Fluids* **27**, 2956 (1984).
- ⁶C. P. Ritz, R. V. Bravenec, P. M. Schoch, R. D. Bengtson, J. A. Boedo, J. C. Forster, K. W. Gentle, Y. He, R. L. Hickok, Y. J. Kim, H. Lin, P. E. Phillips, T. L. Rhodes, W. L. Rowan, P. M. Valanju, and A. J. Wootton, *Phys. Rev. Lett.* **62**, 1844 (1989).
- ⁷C. P. Ritz, H. Lin, T. L. Rhodes, and A. J. Wootton, *Phys. Rev. Lett.* **65**, 2543 (1990).
- ⁸G. Van Oost, J. Adámek, V. Antoni, P. Balan, J. A. Boedo, P. Devynck, I. Duran, L. Eliseev, J. P. Gunn, M. Hron, C. Ionita, S. Jachmich, G. S. Kirnev, E. Martines, A. Melnikov, R. Schrittwieser, C. Silva, J. Stöckel, M. Tendler, C. Varandas, M. Van Schoor, V. Vershkov, and R. R. Weynants, *Plasma Phys. Controlled Fusion* **45**, 621 (2003).
- ⁹C. Hidalgo, M. A. Pedrosa, and B. Gonçalves, *New J. Phys.* **4**, 51 (2002).
- ¹⁰P. Devynck, J. Stöckel, J. Adámek, I. Dcaronuran, M. Hronm, and G. Van Oost, *Czech. J. Phys.* **53**, 853 (2003).
- ¹¹I. C. Nascimento, Yu. K. Kuznetsov, J. H. F. Severo, A. M. M. Fonseca, A. Elfimov, V. Bellintani, M. Machida, M. V. A. P. Heller, R. M. O. Galvão, E. K. Sanada, and J. I. Elizondo, *Nucl. Fusion* **45**, 796 (2005).
- ¹²I. C. Nascimento, Yu. K. Kuznetsov, Z. O. Guimarães-Filho, I. El Chamaa-Neto, O. Usuriaga, A. M. M. Fonseca, R. M. O. Galvão, I. L. Caldas, J. H. F. Severo, I. B. Semenov, M. V. A. P. Heller, V. Bellintani, J. I. Elizondo, and E. Sanada, *Nucl. Fusion* **47**, 1570 (2007).
- ¹³C. Silva, I. Nedzelskiy, H. Figueiredo, J. A. C. Cabral, C. A. F. Varandas, and J. Stoeckel, *Czech. J. Phys.* **55**, 937 (2003).
- ¹⁴R. R. Weynants and G. Van Oost, *Plasma Phys. Controlled Fusion* **35**, 177 (1993).
- ¹⁵R. R. Weynants, *J. Plasma Fusion Res.* **4**, 3 (2001).
- ¹⁶G. Van Oost, J. P. Gunn, A. Melnikov, J. Stöckel, and M. Tendler, *Czech. J. Phys.* **51**, 957 (2001).
- ¹⁷F. Wagner, G. Becker, K. Behringer, D. Campbell, A. Eberhagen, W. Engelhardt, G. Fussmann, O. Gehre, J. Gernhardt, G. v. Gierke, G. Haas, M. Huang, F. Karger, M. Keilhacker, O. Klüber, M. Kornherr, K. Lackner, G. Lisitano, G. G. Lister, H. M. Mayer, D. Meisel, E. R. Müller, H. Murmann, H. Niedermeyer, W. Poschenrieder, H. Rapp, H. Röhr, F. Schneider, G. Siller, E. Speth, A. Stäbler, K. H. Steuer, G. Venus, O. Vollmer, and Z. Yü, *Phys. Rev. Lett.* **49**, 1408 (1982).
- ¹⁸R. J. Groebner, K. H. Burrell, and R. P. Seraydarian, *Phys. Rev. Lett.* **64**, 3015 (1990).
- ¹⁹K. Ida, H. Hidekuma, Y. Miura, T. Fujita, M. Mori, K. Hoshino, N. Suzuki, T. Yamauchi, and JFT-2M Group, *Phys. Rev. Lett.* **65**, 1364 (1990).
- ²⁰H. Biglari, P. H. Diamond, and P. W. Terry, *Phys. Fluids B* **2**, 1 (1990).
- ²¹K. H. Burrell, *Phys. Plasmas* **4**, 1499 (1997).
- ²²A. S. Ware, P. W. Terry, B. A. Carreras, and P. H. Diamond, *Phys. Plasmas* **5**, 173 (1998).
- ²³J. C. Perez, W. Horton, R. D. Bengtson, and T. Carter, *Phys. Plasmas* **13**, 055701 (2006).
- ²⁴D. del Castillo-Negrete and P. J. Morrison, *Phys. Fluids A* **5**, 948 (1993).
- ²⁵D. del Castillo-Negrete and P. J. Morrison, "Hamiltonian chaos and transport in quasigeostrophic flows," in *Chaotic Dynamics and Transport in Fluids and Plasmas*, edited by I. Prigogine (American Institute of Physics, New York, 1993), p. 181.
- ²⁶W. Horton, *Plasma Phys. Controlled Fusion* **27**, 937 (1985).
- ²⁷J. Moser, *Nachr. Akad. Wiss. Goett. II, Math.-Phys. Kl.* **IIa**, 1 (1962).
- ²⁸D. del Castillo-Negrete, *Phys. Plasmas* **7**, 1702 (2000).
- ²⁹D. del Castillo-Negrete, J. M. Greene, and P. J. Morrison, *Physica D* **91**, 1 (1996).
- ³⁰D. del Castillo-Negrete, J. M. Greene, and P. J. Morrison, *Physica D* **100**, 311 (1997).
- ³¹D. del Castillo-Negrete and P. J. Morrison, *Bull. Am. Phys. Soc.* **37**, 1547 (1992).
- ³²P. J. Morrison, *Phys. Plasmas* **7**, 2279 (2000).
- ³³M. N. Rosenbluth, R. Z. Sagdeev, J. B. Taylor, and G. M. Zaslavsky, *Nucl. Fusion* **6**, 297 (1966).
- ³⁴J. M. Finn, *Nucl. Fusion* **15**, 845 (1975).
- ³⁵W. Horton, H.-B. Park, J.-M. Kwon, D. Strozzi, P. J. Morrison, and D.-I. Choi, *Phys. Plasmas* **5**, 3910 (1998).
- ³⁶J. M. Kwon, W. Horton, P. Zhu, P. J. Morrison, H.-B. Park, and D. I. Choi, *Phys. Plasmas* **7**, 1169 (2000).
- ³⁷J. S. E. Portela, I. L. Caldas, R. L. Viana, and P. J. Morrison, *Int. J. Bifurcation Chaos Appl. Sci. Eng.* **17**, 1589 (2007).
- ³⁸M. Roberto, E. C. da Silva, I. L. Caldas, and R. L. Viana, *Phys. Plasmas* **11**, 214 (2004).
- ³⁹W. Horton, *Plasma Phys.* **23**, 1107 (1981).
- ⁴⁰R. G. Kleva and J. F. Drake, *Phys. Fluids* **27**, 1686 (1984).
- ⁴¹F. A. Marcus, T. Kroetz, M. Roberto, I. L. Caldas, E. C. da Silva, R. L. Viana, and Z. O. Guimarães-Filho, *Nucl. Fusion* **48**, 024018 (2008).
- ⁴²I. Osipenkov, "Diffusion in chaotic systems," Senior dissertation, Department of Physics, The University of Texas at Austin, 2000.
- ⁴³R. M. O. Galvão, Yu. K. Kuznetsov, I. C. Nascimento, E. Sanada, D. O. Campos, A. G. Elfimov, J. I. Elizondo, A. N. Fagundes, A. A. Ferreira, A. M. M. Fonseca, E. A. Lerche, R. Lopez, L. F. Ruchko, W. P. de Sá, E. A. Saettone, J. H. F. Severo, R. P. da Silva, V. S. Tsypin, R. Valencia, and A. Vannucci, *Plasma Phys. Controlled Fusion* **43**, 1181 (2001).
- ⁴⁴D. del Castillo-Negrete, *Phys. Fluids* **10**, 576 (1998).
- ⁴⁵F. Alberto Marcus, "Particle transport induced by drift waves," Ph.D. thesis, Institute of Physics, University of São Paulo, 2007.
- ⁴⁶I. C. Nascimento, I. L. Caldas, and R. M. O. Galvão, *J. Fusion Energy* **12**, 529 (1993).
- ⁴⁷M. V. A. P. Heller, R. M. Castro, I. L. Caldas, Z. A. Brasília, R. P. Silva, and I. C. Nascimento, *J. Phys. Soc. Jpn.* **66**, 3453 (1997).
- ⁴⁸M. V. A. P. Heller, I. L. Caldas, A. A. Ferreira, E. A. O. Saettone, and A. Vannucci, *J. Plasma Phys.* **73**, 295 (2007).
- ⁴⁹I. L. Caldas, F. A. Marcus, A. M. Batista, R. L. Viana, S. R. Lopes, M. V. A. P. Heller, Z. O. Guimarães Filho, P. J. Morrison, and W. Horton, *AIP Conf. Proc.* **875**, 341 (2006).
- ⁵⁰R. M. Castro, "Turbulence control in tokamak TBR-1," Ph.D. thesis, Institute of Physics, University of São Paulo, 1996.
- ⁵¹A. A. Ferreira, M. V. A. P. Heller, I. L. Caldas, E. A. Lerche, L. F. Ruchko, and L. A. Baccalá, *Plasma Phys. Controlled Fusion* **46**, 669 (2004).
- ⁵²J. L. Tennyson, J. D. Meiss, and P. J. Morrison, *Physica D* **71**, 1 (1994).